Wind-tunnel modelling of the tip-speed ratio influence on the wake evolution

Victor P. Stein, Hans-Jakob Kaltenbach

Fachgebiet Strömungsbeeinflussung und Aeroakustik, Fakultät Maschinenwesen
Technische Universität München, Boltzmannstr. 15, 85748 Garching

E-mail: victor.stein@aer.mw.tum.de, hans-jakob.kaltenbach@tum.de

Abstract. Wind-tunnel measurements on the near-wake evolution of a three bladed horizontal axis wind turbine model (HAWT) in the scale 1:$\mathcal{O}(350)$ operating in uniform flow conditions and within a turbulent boundary layer at different tip speed ratios are presented. Operational conditions are chosen to exclude Reynolds number effects regarding the turbulent boundary layer as well as the rotor performance. Triple-wire anemometry is used to measure all three velocity components in the mid-vertical and mid-horizontal plane, covering the range from the near- to the far-wake region. In order to analyse wake properties systematically, power and thrust coefficients of the turbine were measured additionally. It is confirmed that realistic modelling of the wake evolution is not possible in a low-turbulence uniform approach flow. Profiles of mean velocity and turbulence intensity exhibit large deviations between the low-turbulence uniform flow and the turbulent boundary layer, especially in the far-wake region. For nearly constant thrust coefficients differences in the evolution of the near-wake can be identified for tip speed ratios in the range from 6.5 to 10.5. It is shown that with increasing downstream distances mean velocity profiles become indistinguishable whereas for turbulence statistics a subtle dependency on the tip speed ratio is still noticeable in the far-wake region.

1. Introduction

A good understanding of the near-wake evolution in different environmental conditions is essential for the optimization of power production and load alleviation of densely spaced clusters of wind turbines. Several investigations focused on the modelling of the near wake evolution of scale wind turbine models in uniform flow conditions ([1], [2], [3]). They found that the velocity distribution in the wake, its expansion and phenomenons like wake meandering and its frequency are strongly influenced by the wind turbine thrust and its tip speed ratio (TSR) $\lambda = \Omega R/U_{hub}$, where R denotes the rotor radius, Ω the angular frequency and U_{hub} the (undisturbed) mean velocity at hub height. Others focused on modelling the interaction of wind turbine wakes with the atmospheric boundary layer. Aubrun [4] showed that the wake of a rotating model and a porous disc developing in the modelled atmospheric boundary layer are indistinguishable after 3 rotor diameters downstream of the rotor discs, whereby the porous disc was designed to match the velocity deficit in the wake of the rotor at a downstream distance of 0.5 rotor diameters. Recently, Bastankhah [5] studied the interaction between the wake of a small scale wind turbine model and a turbulent boundary layer for different TSRs and yaw angles. He showed that the near wake region is significantly influenced by the TSR of the turbine and the wake rotation.

All mentioned studies on small scale model wind turbines, with a rotor diameter of $D =$

$2R < 0.5$m, operating within turbulent boundary layers were limited to TSRs lower than 7, and as far as stated, designed for TSRs lower than 4 whereas full-scale wind turbines are designed for TSRs around 7 [6]. This mismatch can be considered to be a result of limitations regarding achievable Reynolds numbers in wind tunnel modelling. For low chord based Reynolds numbers airfoils exhibit a low efficiency (lift to drag ratio), which in result leads to a lower maximum power coefficient at a lower design TSR compared to full-scale wind turbines [6]. Furthermore, since the wind varies the turbine does not always operate at the design TSR, the actual value depending on the dynamics of the wind changes and on the properties of the control system. For example, overspeeding results when the torque requested by the generator is lower than the torque produced by the turbine in case of a sudden increase wind speed in gust. Up to now it is not entirely clear to what degree a mismatch of TSR between physical scale model and full scale affects the wake evolution of a turbine operating in a turbulent boundary layer.

Thus, the study compares the near-wake evolution in a low-turbulence uniform approach flow and within a turbulent boundary layer at different TSRs. Primary goal is a quantitative assessment of the changes in mean velocity and turbulence statistics in the near and far wake that occur when the TSR and the power coefficient changes while the thrust coefficient remains nearly constant.

2. Experimental Set-up

2.1. Wind Tunnel and Instrumentation

The experiments are performed at the chair of aerodynamics closed-loop boundary layer wind tunnel. The test section is 2.7 m wide, 1.8 m high and 21 m long. Flow uniformity at the nozzle outlet is achieved by means of a honeycomb, four sets of screens and a section with a contraction ratio of 2.12:1. At the nozzle the free stream turbulence level is 0.3%. An atmospheric boundary layer is simulated using Counihan's technique [7], where different arrangements of vertical fins, vortex generators and distributed roughness on the wind tunnel floor result in a family of mean flow profiles $U(z) \sim z^{\alpha}$ characterized by certain values of shear exponent α and roughness length z_0 [8]. Instantaneous velocities are measured using a triple hot-wire probe which is made of 5μm gold-coated tungsten wires of 3mm length. The probe is connected to a ten-channel AALAB AN 1003 anemometer system. Each channel consists of a Wheatstone bridge, an amplifier and a low-pass filter with a 1kHz cut-off frequency. Velocity signals are sampled at 3 kHz using a 12-bit digitizer Data Translation DT2821 with a record length of 30 s. With this configuration a relative error of the velocity measurement of $\epsilon_u < 3\%$ is obtained, see [9]. The mean velocity at hub height U_{hub} is measured simultaneously by means of a Prandtl tube, located at a position upstream of the wind turbine at which no flow displacement due to the turbine itself is noticeable.

2.2. Boundary Layer Characteristics

In the current study, the wind turbine model is located approximately 12.5 meters downstream of the fins where the boundary layer thickness is $\delta \approx 1.5$ m. For the applied distribution of roughness elements, consisting of staggered columns of Lego bricks with a height of $h_r = 4.75$cm and an average spacing of $\Delta s = 30$cm, the parameters $\alpha = 0.16$ and $z_0 = 0.53$mm were determined by fitting a logarithmic and a power law velocity profile to the measured average velocity $\bar{u}$. Additionally the friction velocity u_τ is estimated by the fitting as $u_\tau/U_{hub} = 0.061$. At a scale of 1:$\mathcal{O}(350)$ these parameters correspond to a neutrally stratified boundary layer over farm land. Figure 1 shows the vertical profiles of the a) mean velocity, b) turbulence intensity and c) shear stress measured in the boundary layer using $z_{hub} = 450$mm and $U_{hub} = 10.8$m/s as reference. Additionally, in figure c) the longitudinal length scales are compared with Counihans empirical expression $L_u^x = Cz^{\alpha}$ [10]. The results show, that the scales in the wind tunnel follow the correct trend up to half of the hub height z_{hub}. Above this region length scales decrease slightly in size reaching a constant value. At the upper edge of the rotor disc the relative error

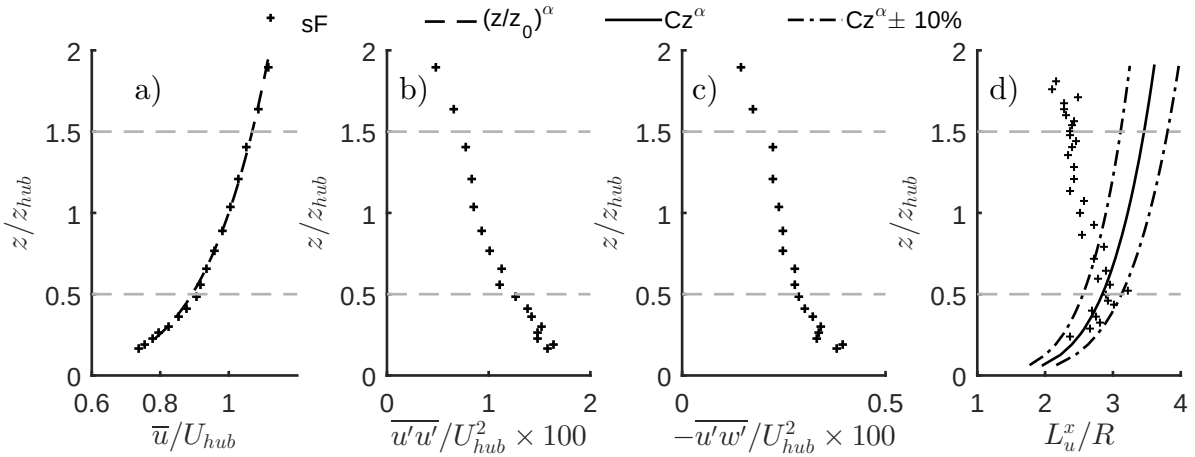

Figure 1. a) mean velocity in axial direction $\overline{u}$, b) axial turbulence intensity $\overline{u'u'}$ and c) shear stress $\overline{u'w'}$ within the turbulent boundary layer, all normalised by the mean velocity at hub height U_{hub}. d) longitudinal integral length scale L_u^x normalised by the rotor radius R. Horizontal *dashed lines* indicate the rotor edges.

regarding the empirical expression is about 30%. Despite this fact the model scale was chosen to assure Reynolds number independence of main flow statistics and a realistic rotor performance.

Throughout all presented measurements the roughness Reynolds number, $Re_\tau = u_\tau z_0/\nu$, where u_τ is the friction velocity and ν the kinematic viscosity, is between $Re_\tau = 13 - 22$ which falls well above the lower limit of 1 suggested by Heist and Castro [11]. Hence the surface can be considered as aerodynamically rough and main flow statistics should be independent of Reynolds number. Chamorro et al. [12] suggest a Reynolds number independence of the wake of a model wind turbine on the basis of the rotor diameter D at $Re_D = U_{hub}D/\nu > 9.3 \times 10^4$. For the measurements presented here Reynolds numbers are also above this limit, ranging from $Re_D = 1.88 \times 10^5 - 3.04 \times 10^5$.

2.3. Model Wind Turbine Design & Characteristics

The wind turbine model is a three-bladed HAWT with a rotor diameter of $D = 450$ mm and equal hub height $z_{hub} = D$. At the considered scale of 1:$\mathcal{O}(350)$ it represents a multi megawatt wind turbine with a rotor diameter of 160m. Blocking effects are considered to be negligible since the blockage ratio of the rotor is 3.3% (i.e., the ratio of the blade swept area to the tunnel cross section area). The blade profile of the rotor is the SD7003 low Reynolds number airfoil [13]. The rotor is designed for a TSR of $\lambda_{dsgn} = 6.5$, chord and twist distribution, shown in Figure 2 were obtained by applying a so called 'optimal design for variable speed operation' [6]

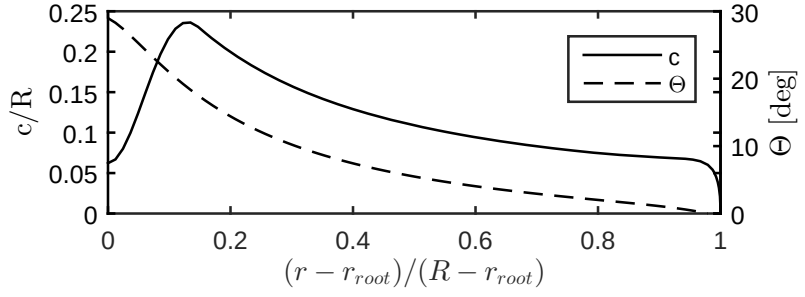

Figure 2. *Solid line* gives chord and *dashed line* twist distribution, where r denotes the radial position and r_{root} the radius of the blade root.

Table 1. Rotor performance within low-turbulence uniform approach flow (uF) and turbulent boundary layer (sF) for different TSR λ. C_P includes estimate on bearings friction. ΔC_P denotes reduction if estimate is excluded.

	U_{hub}	uF		sF		
λ	[m/s]	C_P	C_T	C_P	C_T	ΔC_P
6.5	10.8	0.396	0.76	0.415	0.76	0.032
9.0	7.8	0.285	0.74	0.316	0.80	0.082
10.5	6.7	0.140	0.76	0.179	0.77	0.130

Figure 3. Picture of the turbine model

for which the angle of attack at the design TSR is almost constant $\alpha = 4°$ along the blade. For all measurements presented here a blade pitch angle of 2° was chosen. The rotor is mounted on a shaft which is connected via a clutch with a DC-generator to extract the energy from the wind. Generator and nacelle are cylindrical shaped and have a diameter of 40mm, whereas the tower, a circular cross-section tube, has a diameter of 20mm. The angular frequency Ω of the rotor is kept constant by a four-quadrant controller during the measurements with a standard deviation of $< 0.25\%$. Generated torque is *estimated* from the electric current of the generator while the thrust is *measured directly* by means of a strain gauge installed between nacelle and tower. Thus, thrust includes axial component of forces on the blades, spinner and nacelle. A photo of the wind turbine model is shown in Figure 3.

Measurements will be presented for TSRs λ in low-turbulence uniform approach flow (uF) and within a turbulent boundary layer (sF). TSRs are listed in Table 1 along with the mean flow velocity at hub height U_{hub} and the associated power and thrust coefficients

$$C_P = \frac{Q\Omega}{1/2\rho U_{hub}^3 \pi R^2} \qquad \text{and} \qquad C_T = \frac{T}{1/2\rho U_{hub}^2 \pi R^2} \tag{1}$$

where Q is the generated torque at the rotor, T the thrust and ρ the air density. Power and thrust coefficients measured during the experiments are also depicted in Figure 4. Additionally

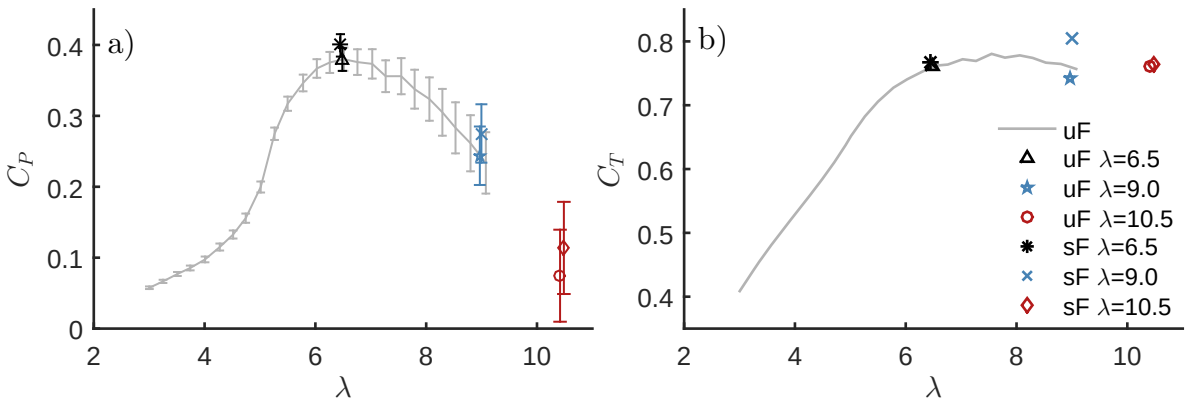

Figure 4. a) Power and b) thrust coefficients as function of TSR λ for constant chord based Reynolds number $\bar{Re}_c = 62500$. *Line* denotes rotor performance in low-turbulence uniform approach flow. *Legend* gives flow conditions and TSR for which hot-wire measurements were performed.

a performance curve covering TSRs from $\lambda = 3 - 9$ recorded within low-turbulence uniform flow conditions is given.

Rotor performance at small model scales is known to be quite sensitive to changes in Reynolds number. For this type of blade design and uniform flow conditions the chord based Reynolds number is almost constant along the blade for the design TSR and higher values at $Re_c \approx 62500$, except towards the tip and root. However, within sheared flow the chord based Reynolds number is a function of the azimuthal angle and radial position. Therefore, by adapting the angular frequency Ω and flow velocity at hub height U_{hub} accordingly, as given in Table 1, Reynolds number dependency on the TSR can be excluded for all cases.

Due to the decrease in freestream velocity with increasing TSR, the generated torque drops to a level in the order of the losses caused by the bearings friction. Hence, an estimate on the bearings friction can be incorporated in the calculation of the power coefficient by adding the electric current which is necessary to run the generator without attaching the rotor. In table 1 power coefficients C_P are calculated by including the estimate while ΔC_P denotes the contribution of the estimate. In Figure 4a) lower and upper values of the power coefficient C_P are calculated by neglecting or incorporating the estimate on the bearings friction respectively. A discussion on the validity of the estimate on the bearings friction is given in section 3.1. For all three TSRs the wind turbine exhibits an almost constant thrust coefficient of about $C_T = 0.77 \pm 0.03$, whereas the power coefficient C_P decreases from its maximum value to small values. Hence, deviations in the wake should only be caused by changes in the TSR or the local torque and thrust distribution.

3. Results

3.1. Effect of tip speed ratio on axial and azimuthal mean velocity

Figure 5 shows the spatial distribution of the averaged axial velocity component $\overline{u}_x$. In this and all following figures a) denotes the mid-vertical and b) the mid-horizontal plane. Two sets of curves are shown in both plots, including results for a low-turbulence uniform approach flow and for a turbulent boundary layer. Due to less mixing as a result of lower upstream turbulence the first group exhibits a more pronounced wake at the blade tips and slower recovery of the wake deficit. For both sets of curves deviations can be seen in between different TSRs. As mentioned before in all cases the wind turbine exhibits an almost constant thrust coefficient C_T. Therefore deviations between TSRs must be explained by considerations regarding the rotor aerodynamics. With increasing TSR the angle of attack at the inward section of the blades is decreased, resulting in a lower contribution to the thrust. At the outward section the increasing velocity of the relative wind results in an increasing contribution to the thrust towards the tip. From the figure this effect can clearly be seen in the vicinity of the rotor ($x/R = 2$), where an increase of $\overline{u}_x$ with TSR is observed in the inner region and a decrease in the outer region of the rotor. Due to the high ambient turbulence in the case of the turbulent boundary layer this effect is already less pronounced in the vicinity of the rotor and vanishes in the outer region for a downstream distance of $x/R = 6$. For distances of $x/R \geq 10$ the different profiles become indistinguishable, whereas in the low-turbulence uniform approach flow differences persist over the whole measured range. For these cases the flow below the rotor does not reach the free stream velocity over the whole measured range as it is the case for the region above the rotor. This is probably caused by the presence of the tower.

Figure 6 shows the spatial distribution of averaged azimuthal velocity component $\overline{u}_\psi$. As already seen for the axial velocity component, also the azimuthal velocity component in the turbulent boundary layer cases recovers much faster to its undisturbed level compared to the cases in low-turbulence flow condition. Again, deviations in between different TSRs can clearly be identified, especially in the vicinity of the rotor, where cases in the turbulent boundary layer and in the low-turbulence flow exhibit quite similar distributions. In contrast to the

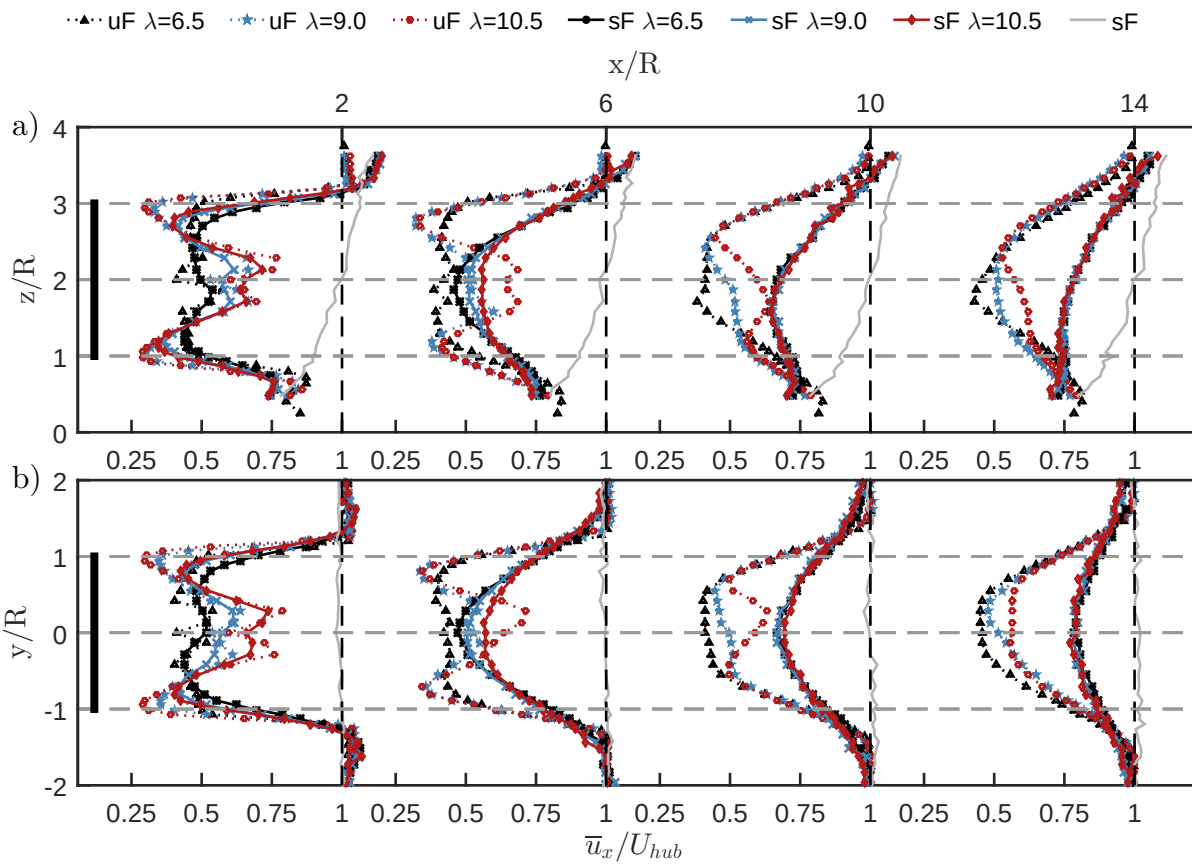

Figure 5. Profiles of mean axial velocity component $\overline{u}_x$ in the a) mid-vertical and b) mid-horizontal plane at axial positions x/R =2, 6, 10, 14. In this and all following figures low-turbulence uniform approach flow conditions are denoted by *full lines*, turbulent boundary layer conditions by *dotted lines*. The *legends* above the diagrams indicate flow conditions and TSR for each profile.

almost constant thrust coefficient C_T, the power coefficient C_P drops from its maximum value to small values with increasing TSR, see Figure 4(a). Since the rotation of the wake is directly connected with the power coefficient C_P, the decrease of azimuthal velocity is to be expected. For the case in low-turbulence flow conditions at a TSR of $\lambda = 10.5$ the measured power coefficient without incorporating the estimate on the bearings friction exhibits a value close to zero. Hence, wake rotation should not occur, but this is clearly not the case. Knowing the axial and azimuthal velocity distribution in the wake, torque generated by the rotor can be approximated by integrating the angular momentum flux crossing a reference surface in the vicinity of the rotor according to

$$Q = -\int_A \rho(\overline{u}_x\overline{u}_\psi + \overline{u'_x u'_\psi})r\,dA\,. \tag{2}$$

From this, estimates of power coefficients in the low-turbulence approach flow are obtained as $C_P = 0.381$, 0.296 and 0.155 for TSRs of $\lambda = 6.5$, 9.0 and 10.5 respectively. These values are within some percent of the measured power coefficients when the estimate on the bearings friction is incorporated. Therefore, taking this estimate into account seems to be justified.

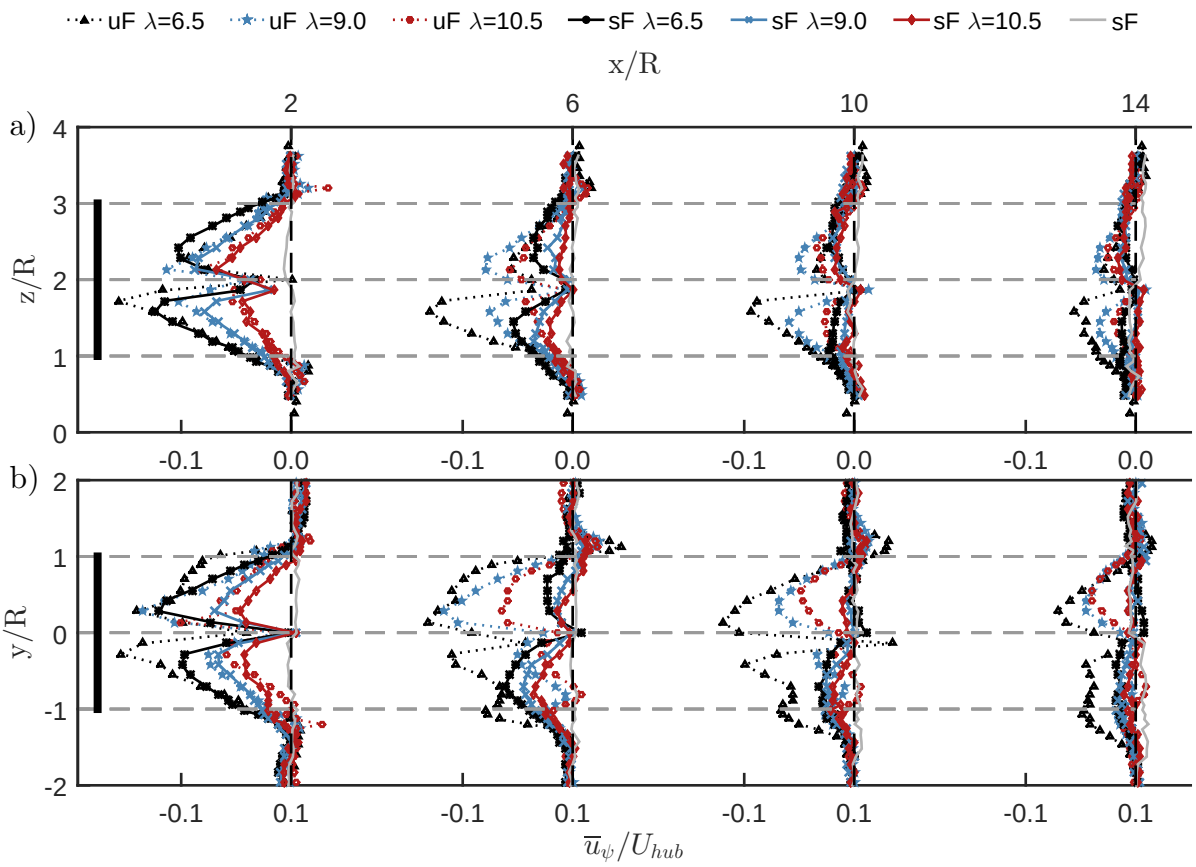

Figure 6. Profiles of mean azimuthal velocity component $\overline{u}_\psi$ in the a) mid-vertical and b) mid-horizontal plane at axial positions x/R =2, 6, 10, 14.

3.2. Effect of tip speed ratio on Reynolds Stresses

The spatial distribution of the shear stress with respect to the radial direction $\overline{u'_x u'_r}$, normalised by the velocity at hub height U_{hub}, is shown in figure 7. Figure 8 and 9 depict the spatial distribution of the turbulence intensities for the velocity components in axial and azimuthal direction, $\overline{u'_x u'_x}$ and $\overline{u'_\psi u'_\psi}$ respectively. Wake recovery is associated with the rate of change of momentum and hence with the radial distribution of the shear stress $\overline{u'_x u'_r}$. In the near wake ($x/R = 2-6$) around the tip region sharp peaks can be observed which in downstream distance become smoother. This leads to the fast recovery in this region seen in figure 5. In the region of the rotor axis the shear stress exhibits a smoother distribution which is also opposite in sign. Therefore, in this region of the near wake the flow velocity remains constant or is even further decreased, depending on the TSR. Due to the lower magnitude of shear stress $\overline{u'_x u'_r}$ and turbulence intensity $\overline{u'_x u'_x}$ in the case of the low-turbulence uniform flow approach the wake recovers slower, compared to the cases in the turbulent boundary layer. In the far wake ($x/R = 10-14$) profiles of the shear stress and turbulence intensity exhibit just small differences for the cases in the turbulent boundary. Since shear stress and turbulence intensity are the driving forces for changes in the axial velocity, this is consistent with the observation of self similar profiles of the mean axial velocity $\overline{u}_x$ in this region.

For the turbulence intensities $\overline{u'_x u'_x}$ and $\overline{u'_\psi u'_\psi}$ (and also $\overline{u'_r u'_r}$, but not shown here) a tip speed ratio dependency can be identified especially in the near wake but also in the far wake region. In the case of the turbulent boundary layer peaks in the vicinity of the rotor at the tip region

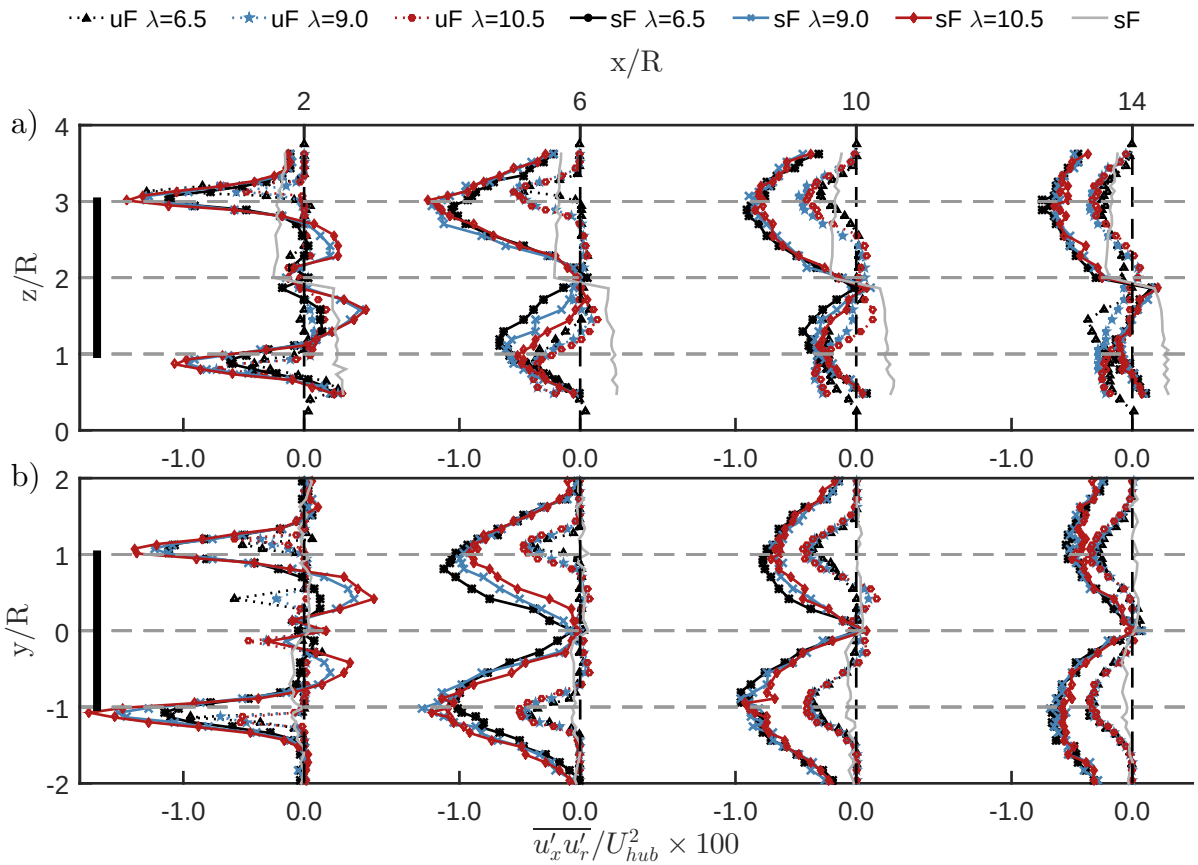

Figure 7. Profiles of Reynolds shear stress $\overline{u'_x u'_r}$, normalised by the velocity at hub height U_{hub}, in the a) mid-vertical and b) mid-horizontal plane at axial positions x/R =2, 6, 10, 14.

increase with increasing TSR λ. This can be explained by the increasing local contribution to the thrust by the tip region which also results in an increased intensity of blade tip vortices. Surprisingly, in the case of the low-turbulence uniform approach flow the trend of the turbulence intensity is rather the other way round. However this statement should be taken with care. Due to the low free stream turbulence intensity steep gradients at $x/R = 2$ occur which results in a low resolution of the effect. At a distance of $x/R = 14$ the turbulence intensity is still higher than for the undisturbed boundary layer, see figure 8 and 9. Even at this distance a TSR dependency is noticeable for the cases in the turbulent boundary layer, especially for the azimuthal turbulence intensity $\overline{u'_\psi u'_\psi}$ where the deviation is more than 20%, see figure 9. From these results it can not be clearly stated whether the observed deviations depend on the TSR itself or rather on the power coefficient and the wake rotation connected with it. However, in both cases the results show that a wind turbine model operating as close as possible to realistic conditions is necessary to predict these subtle changes.

Recently Hancock et al. ([14],[15]) reported a suppression of turbulence intensity just behind the rotor below its undisturbed level. The authors observed this phenomena for measurements within an unstable (suppression of turbulence intensities $\overline{u'_x u'_x}$, $\overline{u'_r u'_r}$) and a neutral boundary layer (just suppression of $\overline{u'_x u'_x}$). Measurements within a stable boundary layer did not exhibit this effect. The authors suggested the phenomena might be a result of a blocking effect of the turbine on the turbulence upstream of the rotor, suppressing $\overline{u'_x u'_x}$. For the measurements in the turbulent boundary layer presented here, this effect is clearly visible in the vicinity of the rotor

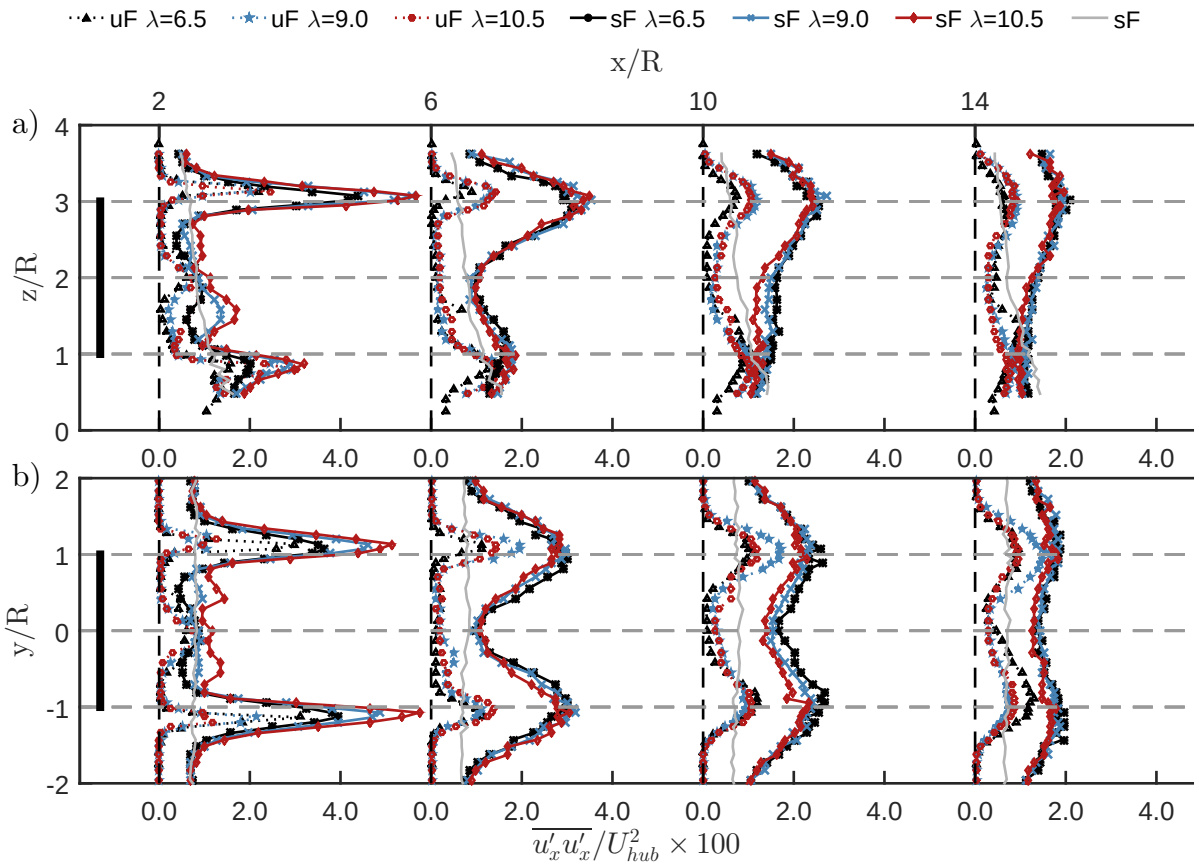

Figure 8. Profiles of axial turbulence intensity $\overline{u'_x u'_x}$, normalised by the velocity at hub height U_{hub}, in the a) mid-vertical and b) mid-horizontal plane at axial positions x/R =2, 6, 10, 14.

mid-section ($x/R = 2$) for the turbulence intensities in axial and azimuthal direction, see figures 8 and 9. For the turbulence intensity $\overline{u'_\psi u'_\psi}$ this phenomena does not exhibit any dependency on the TSR. However, for the axial turbulence intensity $\overline{u'_x u'_x}$ a dependency can clearly be seen. With increasing TSR the turbulence intensity rises from below to values above the undisturbed level.

4. Summary

Wind-tunnel experiments in a 1:$\mathcal{O}(350)$ scale were performed to study the effect of TSR on wind turbine wakes within a turbulent boundary layer and in low-turbulence uniform flow conditions. Triple-wire anemometry was used to characterize the mean velocity in axial and azimuthal direction as well as turbulence intensities of all three velocity components in the wake up to a downwind distance of $x/R = 14$. Presented measurements are considered to be Reynolds number independent and cover TSRs from $\lambda = 6.5 - 10.5$ at which the thrust coefficient is nearly constant and the power coefficient decreases from its maximum to small values.

It is shown that the near-wake is strongly influenced by the tip speed ratio, local thrust distribution and wake rotation. In this region mean velocity distributions within the low-turbulence uniform flow and the turbulent boundary layer are comparable. Due to the different levels of turbulence intensity deviations increase significantly with downstream distance. At a downwind distance of $x/R = 14$ a TSR dependency of the mean velocity can still be noticed in the low-turbulence uniform approach flow, whereas all cases within the turbulent boundary layer

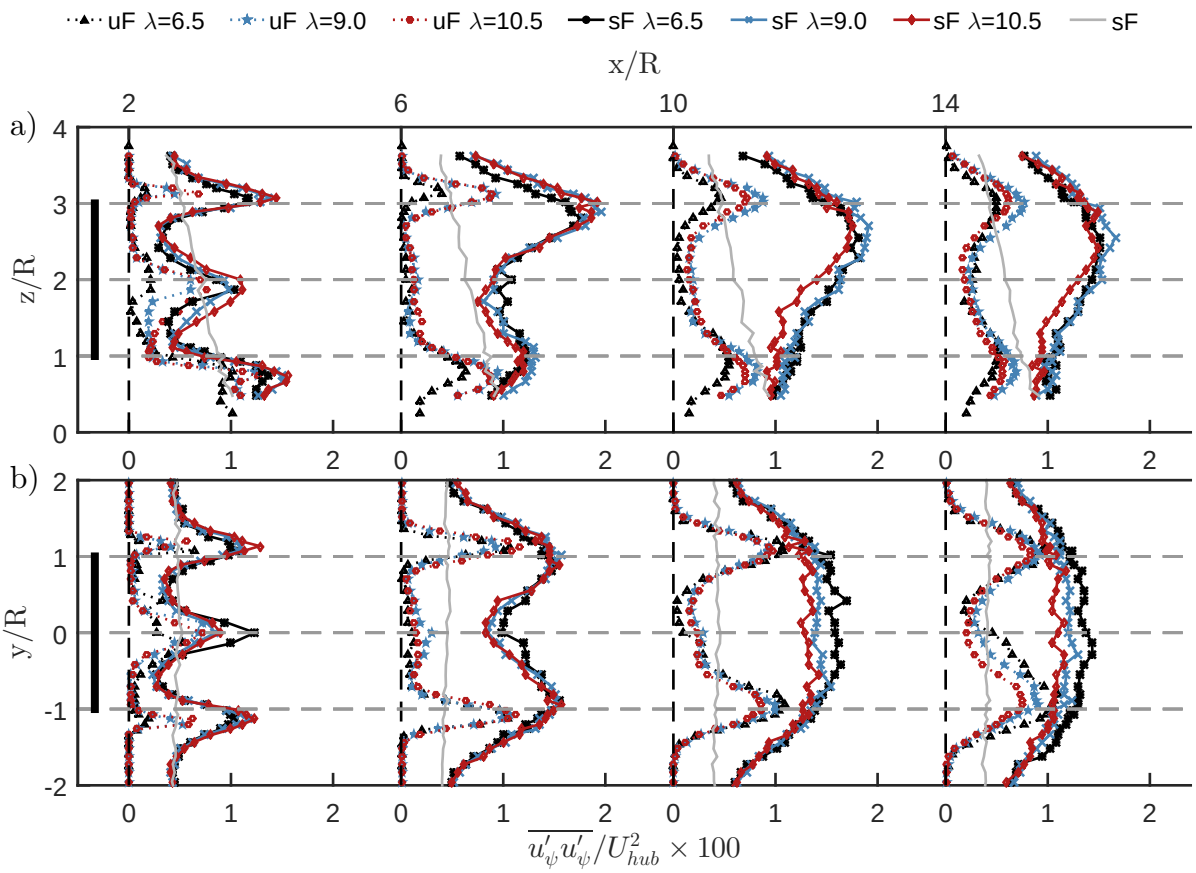

Figure 9. Profiles of azimuthal turbulence intensity $\overline{u'_\psi u'_\psi}$, normalised by the velocity at hub height U_{hub}, in the a) mid-vertical and b) mid-horizontal plane at axial positions x/R =2, 6, 10, 14.

become indistinguishable at a distance of $x/R = 10$. But still, in these cases small differences in turbulence statistics can be noticed even at a distance of $x/R = 14$. In the turbulent boundary layer case a suppression of turbulence intensity in the vicinity of the rotor below the undisturbed level is observed for all three velocity components. For the streamwise turbulence intensity a dependency on the TSR is shown.These findings indicate that for accurate near- and also far-wake predictions based on physical scale models it is preferable to use rotors with design tip speed ratios close to those found in full-scale.

Acknowledgments
This research was supported by the GreenTech Initative of the Eurotech Universities.

References
[1] Krogstad P, Adaramola M 2012 *Wind Energy* **15** 743
[2] Medici D, Alfredsson P 2008 *Wind Energy* **11** 211
[3] McTavish S, Feszty D, Nitzsche F 2013 *J. Wind Eng. Ind. Aerodyn.* **120** 81
[4] Aubrun S, Loyer S, Hancock P, Hayden P 2013 *J. Wind Eng. Ind. Aerodyn.* **120** 1
[5] Bastankhah M, Port-Agel F 2015 *Journal of Physics: Conference Series* **625** 012014
[6] Burton T, Sharpe D, Jenkins N, Bossanyi E 2001 *Wind Energy Handbook* (John Wiley & Sons)
[7] Counihan J 1969 *Atmospheric Environment* **3** 197
[8] Kozmar H 2010 *Theor Appl Climatol* **100** 153

[9] Breitsamter C 1997 *Turbulente Strömungsstrukturen an Flugzeugkonfigurationen mit Vorderkantenwirbeln* (Herbert Utz Verlag)
[10] Counihan J 1975 *Atmospheric Environment* **9** 871
[11] Heist D, Castro I 1998 *Experiments in Fluids* **24** 375
[12] Chamorro L, Arndt R, Sotiropoulos F 2012 *Wind Energy* **15** 733
[13] Selig M, Donovan J, Frase D 1989 *Airfoils at Low Speeds* (H.A. Stokely)
[14] Hancock P, Pascheke F 2014 *Boundary-Layer Meteorol* **151** 23
[15] Hancock P, Zhang S 2015 *Boundary-Layer Meteorol* **156** 395